2024-04

Repeatability of beach morphology change under identical wave forcing

Blenkinsopp, CE

10.1016/j.coastaleng.2024.104485
Coastal Engineering
Elsevier BV

Coastal Engineering 189 (2024) 104485

Contents lists available at ScienceDirect

Coastal Engineering

journal homepage: www.elsevier.com/locate/coastaleng

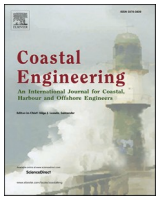

Repeatability of beach morphology change under identical wave forcing

Chris E. Blenkinsopp [a,*], Alan J. Hunter [b], Tom E. Baldock [c], Paul M. Bayle [a,d], Judith Bosboom [d], Daniel Conley [e], Gerd Masselink [e]

[a] Department of Architecture and Civil Engineering, University of Bath, Bath, BA2 7AY, United Kingdom
[b] Department of Mechanical Engineering, University of Bath, Bath, BA2 7AY, United Kingdom
[c] School of Civil Engineering, University of Queensland, St Lucia, Qld, 4072, Australia
[d] Faculty of Civil Engineering and Geosciences, Delft University of Technology, Department of Hydraulic Engineering, P.O. Box 5048, 2600, GA Delft, the Netherlands
[e] Coastal Processes Research Group, School of Biological and Marine Sciences, University of Plymouth, Plymouth, PL4 8AA, United Kingdom

A B S T R A C T

Laboratory investigations of beach morphology change under wave action are undertaken to gain insight into coastal processes, design coastal structures and validate the predictions of numerical models. For the results of such experiments to be reliable, it is necessary that they are repeatable. The equilibrium beach concept, that beach morphology will evolve to a quasi-static equilibrium shape for a given forcing suggests that experiments should be repeatable to some degree. However, sediment transport in turbulent breaking and broken waves is complex and highly variable and the level of repeatability at different temporal and spatial scales is challenging to measure, as such, previous work has restricted comparisons to small numbers of waves. Here we use the results of two identical, 20-h large-scale wave flume experiments to investigate the repeatability of sediment transport and beach morphology change under waves at timescales down to individual swash events. It is shown that while flow characteristics from identical swash events are very repeatable, the sediment transported can be very different in both magnitude and direction due to differences in turbulence, sediment advection and morphological feedback. Over longer periods containing multiple matching swash events however, the beach responds in a very similar manner, with the level of morphological repeatability increasing with time. The results also demonstrate that gross swash zone sediment transport remains high even as a beach profile approaches quasi-equilibrium, but the proportion of individual swash events that cause large sediment fluxes ($>\pm$7.5 kg/event/m) reduces with time. The results of this laboratory study indicate that beach morphology change has a level of determinism over timescales of several minutes and longer, giving confidence in the results from physical modelling studies. However, the large differences in sediment transport from apparently identical swash events questions the value in pursuing numerical predictions of sediment transport at the wave-by-wave timescale unless the reversals in sediment transport between apparently near identical swash events can also be predicted.

1. Introduction

The concept of beach equilibrium, first introduced by Johnson (1920), suggests that, under given wave and water-level forcing, a beach will naturally develop towards a consistent stable profile which corresponds to the "Laboratory" equilibrium definition of Bruun (1954). In reality, a strict equilibrium where sediment transport gradients are zero is not achieved under random waves and profiles reach a state of dynamic equilibrium where sediment is transported with every wave, but the net transport over multiple waves approaches zero and the beach geometry fluctuates around a quasi-equilibrium profile for a given forcing condition (Dean, 2005). Consequently, this concept implies that at the timescales required for quasi-equilibrium (hours to days), the morphology obtained in two identical experiments (scale, wave conditions, water levels, sediment characteristics) should be the same, but with relatively small, time-varying differences due to the expected fluctuations around the quasi-equilibrium profile. Such determinism is important if we are to rely on laboratory experiments to undertake research into beach morphodynamics, validate numerical models or design coastal structures. Evidence for morphological repeatability was recently provided by Eichentopf et al. (2019) and Baldock et al. (2017) who showed through laboratory experiments that for a given forcing condition, the same beach profile shape will develop independent of the initial profile.

While the idea that a beach will develop towards a quasi-stable state appears robust, the details of how a profile evolves towards this state, and the level of repeatability of this process is unclear. Baldock et al. (2017) discussed the existence of morphological hysteresis which suggests that the way in which a beach profile approaches the quasi-equilibrium state is dependent on the beach state and antecedent wave conditions, as well as the current forcing conditions. As part of the same study, Birrien et al. (2018) demonstrated repeatable morphological evolution over durations of order 6-h for a series of storm/recovery cycles with the same wave conditions. Using the results from a

* Corresponding author.
E-mail address: c.blenkinsopp@bath.ac.uk (C.E. Blenkinsopp).

https://doi.org/10.1016/j.coastaleng.2024.104485
Received 19 October 2023; Received in revised form 23 January 2024; Accepted 9 February 2024
Available online 9 February 2024

large-scale wave flume experiment, Eichentopf et al. (2018) demonstrated that an initially planar sand beach forced by 4 h of erosive waves with different time series, but the same statistics evolved in a similar way, but differences in the intermediate and final profiles were evident. Alsina et al. (2016) completed two tests where identical 210-min time series of repeated bi-chromatic waves ($T_G = 15$ s and 27.7 s) were run for slightly different water levels (2.48 m and 2.53 m), starting with an initial 1:15 sand beach slope. Beach profiles were measured at approximately 30-min intervals and indicated very similar profile evolution and cross-shore distributions of sediment transport rate throughout these experiments, with the mean differences between corresponding profiles (1.6 cm) measured through the experiment staying comparable to the difference between the initially constructed profiles (1.04 cm).

Though measurements of profile evolution with repeated wave time series are limited, O'Donoghue et al., 2016. simulated swash events with very repeatable hydrodynamic characteristics on gravel and coarse sand beds using a dam break facility and obtained highly repeatable measurements of intra-swash sediment flux for these idealised flows. Additionally, a series of experiments in the large-scale wave flume facility at the Canal de Investigación y Experimentación Marítima (CIEM), Universidad Politécnica de Cataluña, Barcelona have investigated swash zone hydrodynamics and sediment transport caused by repeated time series of irregular and bi-chromatic waves (Alsina et al. (2012); Cáceres and Alsina (2012); Alsina and Cáceres (2011); Alsina et al., 2016; Alsina et al., 2018; Caceres and Alsina, 2016; van der Zanden et al., 2015; van der Zanden et al., 2019). These studies found tests to be highly repeatable in terms of hydrodynamics (flow depths and cross-shore flow velocities) and observed similar timings and magnitudes of suspended sediment concentration (typically within a factor of two) for corresponding waves. Alsina et al. (2018) and van der Zanden et al. (2015, 2019) also measured intra-swash bed elevation changes and sheet-flow dynamics using a conductivity-based concentration measurement system (CCM+) in repeated bi-chromatic wave groups. A consistent pattern of local erosion during uprush and accretion during backwash with similar timings and magnitudes of the same order for each repeat was observed, though there was considerable scatter in ensemble-averaged intra-swash bed elevation time series, which was substantially more variable than the corresponding depth and velocity time series.

This study will investigate the response of beach profileswith the same initial state to multiple repeats of the same wave forcing over 20 h. The primary focus of the analysis is on the sediment transport and morphology change in the swash zone down to the wave-by-wave timescale, additionally the complete beach profile evolution at the hourly timescale is investigated. This enables the first detailed investigation into the repeatability of morphological evolution at timescales down to individual waves to improve confidence in physical model results and gain understanding of the level of determinism in swash zone sediment transport which has implications for numerical modelling. Furthermore, the results provide new insight into the changing rate of sediment transport caused by the same forcing conditions as a beach approaches a quasi-equilibrium state.

2. Experimental setup and methodology

The data presented here was collected as part of the DynaRev experiment which was completed over a 2-month period from August to September 2017 in the Large Wave Flume (Groβer Wellenkanal, GWK), Hannover, Germany. The primary goal of the experiment was to investigate the resilience of a dynamic cobble berm revetment structure to wave attack and a rising water level (Bayle et al., 2020). The GWK flume is 309 m long, 7 m deep and 5 m wide with a combined piston-flap type wavemaker. All coordinates are given as the distance from the wave paddle rest position ($x = 0$ m) and elevation above the horizontal flume bed ($z = 0$ m).

The complete DynaRev experiment is described in detail by Blenkinsopp et al. (2021) and was conducted in 2 phases (notation is consistent with Blenkinsopp et al., 2021): Phase SB (Sandy Beach) in which a 1:15 planar sand beach ($D_{50} = 0.33$ mm) was monitored as it evolved under a total of 55 h of constant wave forcing ($H_s = 0.8$ m, $T_p = 6.0$ s) with the water level being increased by 0.4 m in 0.1 m increments; and Phase DR (Dynamic Revetment) which also started using a 1:15 planar beach and used identical wave and water level conditions, but included the installation of a dynamic revetment at the berm location after 20 h of waves. Critical to this study, the first 20 h of both Phase SB and DR (denoted Phase SB0 and Phase DR0 in Bayle et al. (2020) and Blenkinsopp et al. (2021)) were identical, with an initially plane 1:15 sand slope at the same distance from the wave paddle being subjected to 10 repetitions of an identical 2-h time series and a constant water level, $z_{WL} = 4.5$ m. Both Phase SB0 and DR0 were divided into a series of 14 identical "runs" with increasing durations as the experiment progressed ranging from 20 min to 3 h. Between each run, waves were ceased to enable measurements of the complete beach profile using a mechanical profiler with a vertical accuracy of 1–2 cm. In this paper, only data from Phases SB0 and DR0 will be analysed, and these phases will be denoted "Experiment SB" and "Experiment DR" here. There was a substantial effort to ensure that the initial 1:15 beach profiles were as identical as possible given the time available, however it should be noted that perfectly reproducing the exact geometry in the same location is near-impossible in a large-scale flume and there were differences in the levels of saturation and compaction. The maximum error between the profiles at the start of experiments SB and DR was 11.0 cm at $x = 241.2$ m, the root mean square error (RMSE) was 4.0 cm and the mean absolute error (MAE) was 3.8 cm, where RMSE and MAE were calculated as:

$$RMSE = \sqrt{\frac{\sum_{i=1}^{N}\left(z_{SB,i} - z_{DR,i}\right)^2}{N}} \tag{1}$$

$$MAE = \frac{1}{N}\sum_{i=1}^{N}\left|z_{SB,i} - z_{DR,i}\right| \tag{2}$$

Where z_{SB} and z_{DR} represent the bed elevation at each cross-shore measurement location for experiments SB and DR respectively and N is the number of measurement locations.

A large suite of instruments was deployed during the experiment to measure waves, morphology, sediment transport and hydrodynamics. The instrumentation is described in full by Blenkinsopp et al. (2021) and only the instruments used to produce the results presented in this paper are detailed below.

An array of three downward-looking SICK LMS511 2D scanning Lidar were mounted in the flume roof ($z = 11.8$ m) at 12 m intervals and used to measure the time-varying water surface elevation and subaerial beach profile along the flume centreline. The Lidar were sampled at a scan rate of 25 Hz and an angular resolution of 0.166° over a 150° field of view. For the results presented here, which focus primarily on swash zone morphology, only the landward-most Lidar at $x = 255$ m was used. Mounted above the swash zone, the Lidar captures the distance to the nearest surface at approximately 740 points between $x = 240$ m (seaward of the maximum rundown limit) and $x = 276$ m (landward of the maximum runup limit), corresponding to the swash surface when a point is submerged or the local bed elevation when it is exposed. For analysis, the data was resampled to a constant spatial resolution of 0.1 m. Using the method described by Bayle et al. (2020), the Lidar dataset was divided into a "bed" and "swash" elevation time series using a variance thresholding technique. This process enables a measurement of the swash zone profile whenever the bed is exposed between swash events (taken as the mean recorded surface elevation between swash events), as well as time series of swash depth corrected for the changing bed morphology throughout the swash zone. The precision of the Lidar measurements of bed elevation was assessed by analysing a 33-min dataset capturing the static sand beach. The bed elevation was assessed every 2 s as the mean measured surface elevation within each time increment at $x = 270$ m. For this dataset, the 1st −99th percentile

range was 1.9 mm indicating a precision of approximately ±0.95 mm.

3. Results

3.1. Beach profile change

Fig. 1 presents the evolution of the submerged and subaerial beach profile measured using the mechanical profiler during the 20-h duration of both experiments. These results confirm that identical wave forcing results in very similar profile evolution throughout the experiments, leading to approximately the same final profile. As discussed in Bayle et al. (2021), the wave forcing led to the development of a breakpoint bar and a smaller inner bar with a consistently higher crest elevation in both experiments and only minor differences in bar locations and

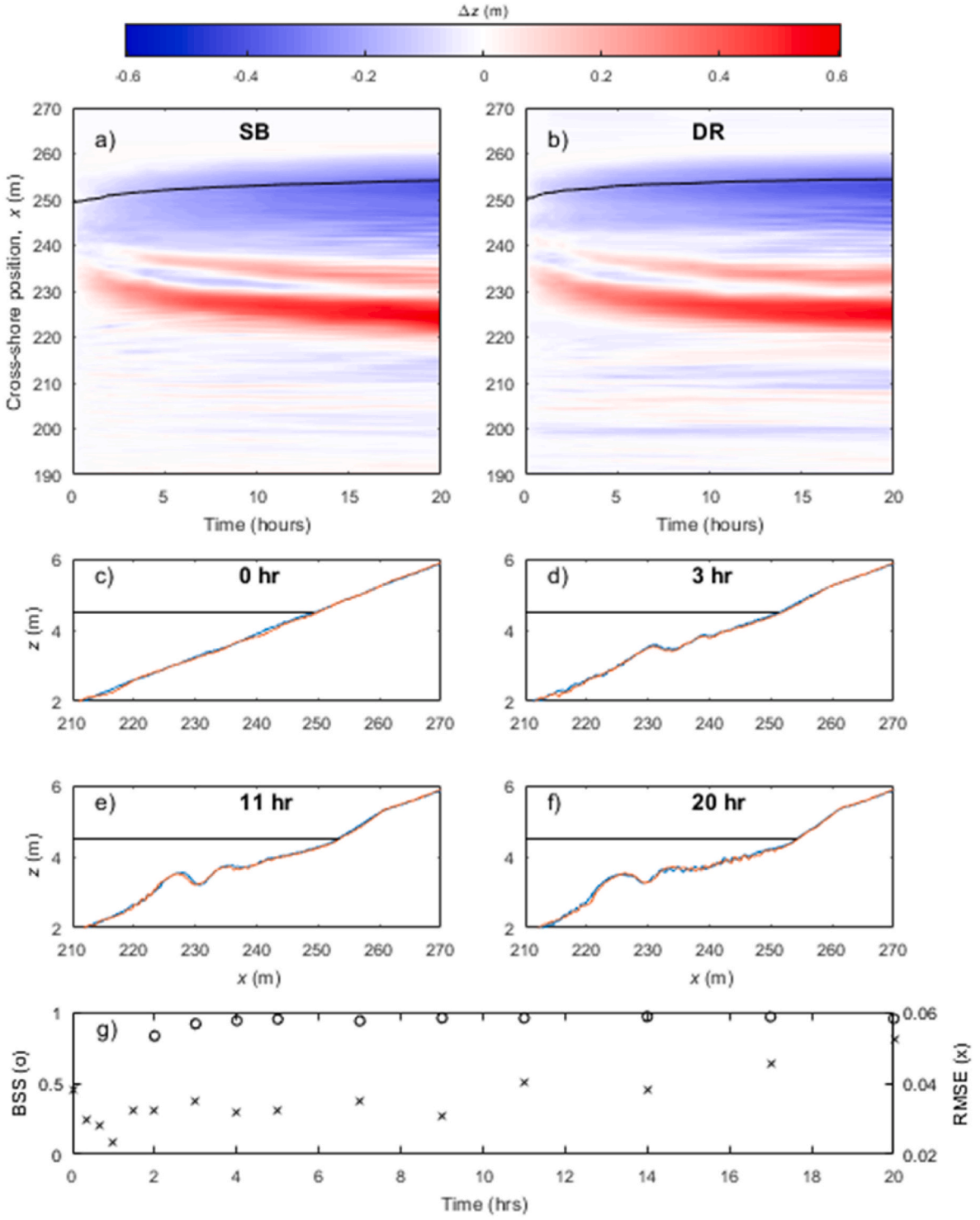

Fig. 1. Beach profile elevation change relative to the initial planar profile for (a) Experiment SB and (b) Experiment DR. The black line indicates the intersection of the SWL (z = 4.5 m) with the profile. (*c*–f) Measured beach profiles at four different times during Experiment SB (blue) and Experiment DR (red)where the black horizontal lines indicate the SWL. (g) Time series of Brier skill score (left axis, black circles) and root mean square error (right axis, black crosses) between equivalent profiles in the two experiments.

elevations (Fig. 1 *d*-f). The observed double-barred profile is characteristic of laboratory experiments using a constant water level (Baldock et al., 2011; Eichentopf et al., 2018; Larson and Kraus, 1989; Masselink et al., 2016), and may be associated with the splash-jet motion of plunging waves pushing material onshore (Dette et al., 2002). Other than small differences in bar geometry, the only notable difference between the experiments is that while sand ripples developed in both experiments on the seaward slope of the primary bar after 1 h of testing and landward of the primary bar after 11 h (Fig. 1 a, b, e, f), the ripple locations were different between experiments. The statistics of the ripple fields (ripple height, η and length, λ) landward of the primary bar (235 m $< x <$ 248 m) were comparable (after 20 h: $\eta_{SB} = 0.178$ m; $\eta_{DR} = 0.185$ m; $\lambda_{SB} = 1.30$ m; $\lambda_{DR} = 1.18$ m), though it should be noted that the ripple height is likely to be consistently underestimated in both experiments because the profiler wheel was too large to follow all ripple troughs. Despite the differences in corresponding profiles caused by the locations of the bed ripples, Fig. 1 g indicates that the RMSE between the profiles in the region between the maximum runup limit ($x = 263$ m) and the seaward limit of profile change ($x = 217$ m) varies little and the value at the end of the experiment (5.3 cm) is comparable to that for the initially constructed profiles of 4.0 cm (Fig. 1 c).

Fig. 1 g provides a time series of the Brier Skill Score (BSS) which has been used to compare the predictions of morphological models (Sutherland et al., 2004a, 2004b; van Rijn et al., 2003). Here, BSS is defined such that it accounts for measurement error (z_e) (Sutherland et al., 2004a):

$$BSS = 1 - \frac{\sum_{i=1}^{N}\left(\left|z_{DR,i} - z_{SB,i}\right| - z_e\right)^2}{\sum_{i=1}^{N}\left(z_{DR,i} - z_{0,i}\right)^2} \tag{3}$$

Where z_0 is the baseline profile, taken here as the mean of the initial (linear) profiles (Sutherland et al., 2004a). Values of BSS for the first 2 h are excluded from Fig. 1 g because changes from the baseline profile are small and of the same magnitude as the difference between profiles for SB and DR leading to unstable values of BSS. For later times, the BSS values remain close to unity, indicating that the profile in experiment DR is a very close approximation to the equivalent profile for SB and vice versa. The BSS decreases very slightly after 11 h when the bed ripples become prominent.

Fig. 1 a and b indicate that the rate of shoreline retreat and net bed elevation change throughout the profile both decrease with time as the beach profile approaches a quasi-equilibrium state with the constant water level and wave forcing conditions (Bruun, 1954; Johnson, 1920). Fig. 2 presents the temporal variation of four morphological indicators obtained from the mechanical profiler measurements over the entire profile that have been used by previous authors (Beuzen et al., 2018; Eichentopf, 2020; Larson, 1988) to assess equilibrium. The results indicate that the rate of absolute beach volume change, shoreline retreat and bar growth and migration is slowing over the course of the experiment, with the rate of change of the latter three potentially approaching zero. However, none of the parameters indicate that quasi-equilibrium has been achieved after 20 h.

3.2. High resolution measurements of swash zone morphology change

The evolution of swash zone morphology captured at the timescale of individual waves by the Lidar array is shown in Fig. 3a and b. It is clear that the spatial distribution and timescales of morphology change are very similar for the two experiments. Note that morphology change in the swash zone was predominantly erosive, with only slight accretion of up to 5 cm in the most landward 3 m of the active profile, where the bed was submerged for less than 5% of the experiment duration.

Time series of bed elevation at three locations were selected according to the percentage of time that they were inundated over the course of the entire 20 h run duration (hereafter denoted $s_{\min}$ where the

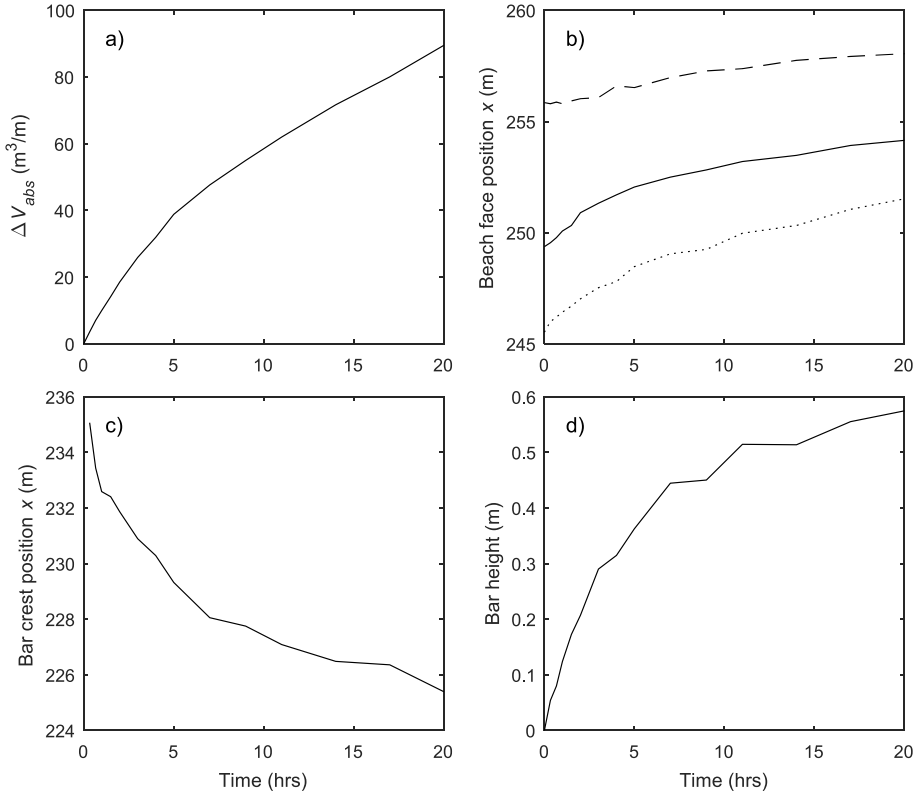

Fig. 2. Temporal evolution of morphological indicators obtained from the mechanical profiler measurements during experiment SB: (a) cumulative absolute change in beach volume landward of x = 200 m. (b) Horizontal position of 3 characteristic points on the beachface: solid line = SWL; dashed line = $R_{2\%}$; dotted line = 2% rundown limit. (c) Cross-shore position of the primary bar crest. (d) Primary bar height measured relative to the initial planar profile.

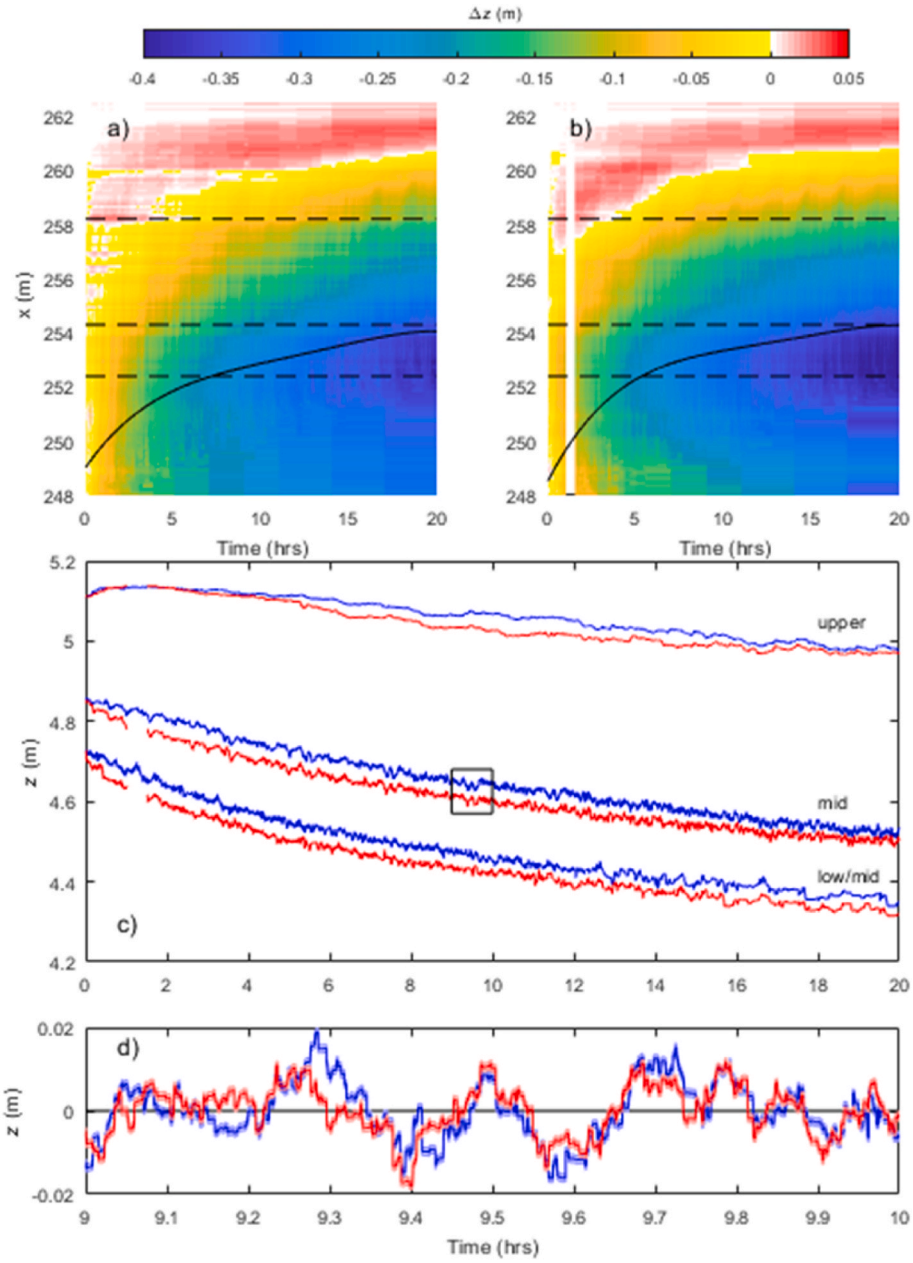

Fig. 3. Swash zone profile change relative to the initial profile for (a) Experiment SB (blue) and (b) Experiment DR (red). Note that due to a data collection problem, no Lidar data was available for Experiment DR between t = 1 h and t = 1 h 30 min. The solid black line indicates the intersection of the SWL with the beach profile at z = 4.5 m. Note that the colour scale indicating erosion/accretion is asymmetric and morphology change in the region presented is almost entirely erosive. (c) Bed elevation at 3 locations on the beachface in the low/mid (x = 252.4 m; s = 80%), mid (x = 254.3 m; s = 50%) and upper (x = 258.2 m; s = 5%) swash zone corresponding to the horizontal dashed lines in (a) for Experiments SB (blue) and DR (red). (d) Detrended (cubic) bed elevation data at x = 254.3 m for the 1-h period indicated by the black square in (c). The error in the bed elevation measurements (±0.95 mm) is shaded.

subscript refers to the number of minutes over which the inundation percentage was calculated) which is an established method of defining relative position within the swash zone (Hughes and Moseley, 2007). The locations were chosen to represent the lower/mid (x = 252.4 m; s_{1200} = 80%), mid (x = 254.3 m; s_{1200} = 50%) and upper (x = 258.2 m; s_{1200} = 5%) parts of the swash zone (3c). The bed elevations presented are the mean of three neighbouring Lidar measurement points to supress the influence of small features such as bed ripples. In the lower and mid swash zone it is observed that the initial bed response for the two experiments is different, due primarily to slightly different initial profiles, as well as different levels of compaction and saturation. However, after approximately 1 h, the bed evolves in a very similar way over the remainder of the experiment and the difference in bed elevation at the same cross-shore position remains approximately constant throughout. In the upper swash zone, the bed evolution during the middle part of the experiment (t = 5–15 h) is slightly different in the two experiments, although the net change over the experiment duration is almost identical. The temporary differences are likely due to the fact that relatively few swashes reach this point in the swash zone and so the variability of the bed elevation is smaller and any differences in bed elevation change from single events can have a longer lasting effect on the bed elevation. By contrast, lower in the swash zone any large differences in bed response from single events are quickly obscured by the response to subsequent swashes. At all three locations shown in Fig. 3c, it is observed that the rate of change of bed elevation is smaller at the end of the experiment than at the start, for example at x = 254.3 m, the rate of

change reduces from −26 mm/h at 2 h to −2.8 mm/h at 20 h. This observation appears to support the concept of beach equilibrium which requires that the rate of morphology change reduces with time as the beach profile approaches quasi-equilibrium with the constant forcing conditions. However, this is obscured by the fact that because the beach is eroding, the relative position of each x-location within the swash zone is changing. For example, while the value of s over the entire 20-h experiment, s_{1200} = 50% at x = 254.3 m, the 20-min value at this cross-shore position varies from s_{20} = 30.9% at the start of the experiment to 78.9% at the end. This reflects the fact that as the beach erodes, this location is more frequently inundated and swash depths increase as time progresses.

Closer inspection of Fig. 3c suggests that in the low and mid swash zone, not only are the overall trends of bed elevation change comparable, but shorter-term changes (O (minutes)) are also very similar, with the same waves leading to a remarkably similar bed response when comparing the two experiments. To highlight this, Fig. 3d shows a shorter time series of bed elevation data after cubic detrending at x = 254.3 m. This figure suggests that while the bed response to the same individual swash events at this single point on the beachface is not necessarily consistent, the changes observed over multiple (O (10)) events are very similar.

The observation that while the sum of change over multiple events is similar, event-by-event changes at a fixed location on the beachface are typically not consistent is confirmed in Fig. 4. The histograms presented in Fig. 4a–d, g indicate that the distribution of bed elevation changes caused by matching individual swash events at each of the selected cross-shore positions for both experiments are very similar. In this analysis, a swash event occurs over the time interval between consecutive detections of 'dry' bed at a defined cross-shore location. Matching swash event are defined as when the arrival and finish times of a swash event are within 1.5 s at the same cross-shore position in both Experiments SB and DR." For both experiments, the distributions are very similar to those presented by Blenkinsopp et al. (2011) and show marked similarities: (1) they are approximately symmetrical at all locations with small negative skewness in the low and mid swash and positive skewness in the upper swash; (2) swash-by-swash bed elevation changes are almost all smaller than ±0.02 m; and (3) the distributions narrow with increasing distance onshore as the mean magnitude of change reduces. Consequently, the integrated effect of these changes leads to the very

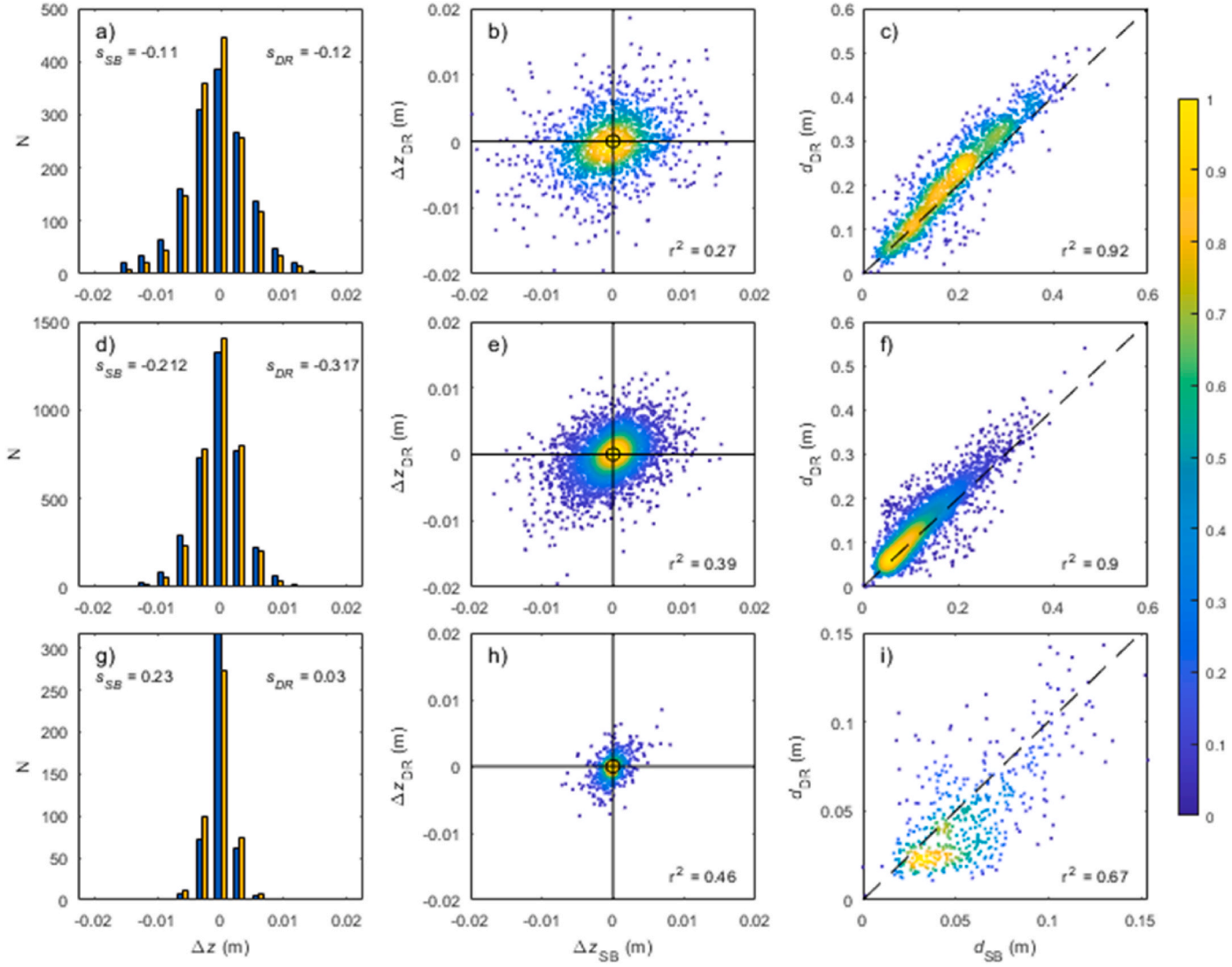

Fig. 4. Left column) Histograms of bed elevation change due to the same swash events for SB (blue) and DR (yellow) at x = 252.4 m (top row), x = 254.3 m (middle row) and x = 258.2 m (bottom row). The skewness (s) for each distribution is shown on the plots. N indicates the number of swash events. Centre column) Scatter plots of event-by-event bed elevation change during SB and DR at x = 252.4 m, 254.3 m and 258.2 m. The circle indicates the estimated uncertainty on bed elevation measurements, ±0.95 mm. Right column) Scatter plots of swash event depth (95th percentile of the swash depth time series) at x = 252.4 m, 254.3 m and 258.2 m. The colour scale indicates the normalised point density for the central and right columns.

similar response of the bed in experiments SB and DR over the experiment duration; however, this similar response is not the result of identical changes in response to individual waves at these locations. Fig. 4b–e and h present scatter plots of the bed elevation change for matched individual swash events and show poor correlation between the individual event-by-event bed elevation changes during experiments SB and DR, while the swash event depths are much more strongly correlated indicating similar hydrodynamic conditions (Fig. 4c–f, i). It is noted that Fig. 4c–f, I indicate a systematic trend of approximately 5% larger depths for matching events in experiment DR, no clear reason can be found for this, however the mean difference is only 1 cm.

Bed elevation changes at a single point on the beachface are expected to be sensitive to the exact relative location within a swash event and this is likely to be different for the same wave in the two experiments due to slight discrepancies in the swash hydrodynamics caused by small differences in beach profile, water level and swash-swash interactions. This may in part explain the lack of close agreement between the bed elevation changes caused by matching swash events in the two experiments (Fig. 4b–d, f and Fig. 3d). Fig. 5a and b presents the measured swash-by-swash bed elevation changes at all locations landward of $x = 254.3$ m for 190 matching swash events detected in both the SB and DR datasets between $t = 9$ and 10 h as presented in Fig. 3d. Note that not all events during this period were able to be matched because in some cases the bed at $x = 254.3$ m remained inundated in one experiment when it was briefly exposed in the other due to small differences in swash hydrodynamics, meaning that the resulting bed elevation changes could not be directly compared. The location analysed, $x = 254.3$ m was chosen because it represents the final shoreline position in both experiments and a consistent number of swash events were observed throughout the experiment even as the beachface moved landward. Inspection of Fig. 5a and b suggests that there is significant cross-shore variability in bed elevation change from a single event and the bed response at locations only 10 cm apart can be quite different. Nonetheless, comparing the same events in SB and DR (Fig. 5a and b), the overall swash zone profile responses to matching events show some similarities with comparable areas of accretion (red) and erosion (blue) within the swash zone, though there is certainly not close agreement.

By integrating the bed elevation changes landward of each measurement point for each event detected at $x = 254.3$ m it is possible to estimate the cross-shore distribution of sediment mass flux on an event-by-event basis for both experiments (see Blenkinsopp et al., 2011). This is considered a more robust method to compare the swash-by-swash changes caused by to the same waves as it is not dependent on a single point measurement. The estimated error in these estimates is 0.5 kg/m/event.

Fig. 5c and d indicate that the transport direction varies from event

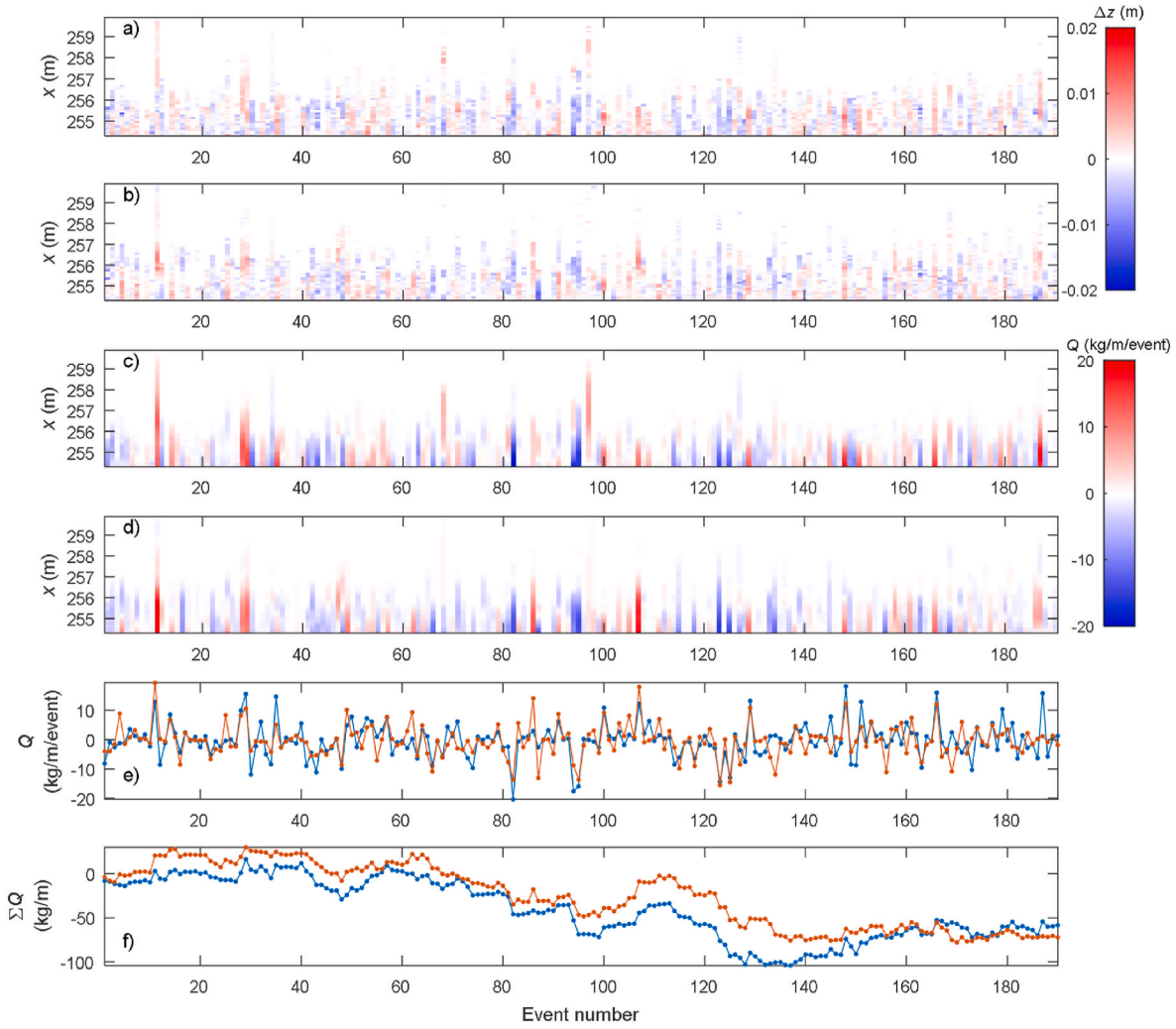

Fig. 5. a and b) Cross-shore distribution of bed elevation change in the swash zone for 190 matching swash events detected at x = 254.3 m between hours 9 and 10 for experiments (a) SB and (b) DR. c and d) Cross-shore distribution of sediment mass flux in the swash zone for 190 matching swash events detected at x = 254.3 m between hours 9 and 10 for experiments (c) SB and (d) DR.I) Mass flux of sediment caused by each matching swash event measured at x = 254.3 m. (f) Cumulative mass flux over the 190 matching events. Blue line indicates results from experiment SB and red is for DR.

to event, but is typically unidirectional within each event, i.e. a swash either causes net landward or net seaward transport of sediment at all measured locations. Furthermore, there is notable similarity between the patterns of transport for the two experiments, with the majority of events (123 of 190) having the same transport direction and comparable magnitudes for this dataset. This is illustrated more clearly in Fig. 5e which shows the event-by-event mass flux at $x = 254.3$ m. At this location the 10th to 90th percentile range of the difference between matching mass fluxes is ±5.9 kg/m/event and the 25th to 75th percentile range is ±2.9 kg/m/event. Fig. 5f presents the cumulative flux for the 190 swash events and demonstrates that while similar fluctuations are observed, a small number of matching events are associated with substantially different sediment fluxes (for example events 4, 95, 134 and 169) and lead to divergence in the cumulative flux time series for the two experiments. Further examination of these events reveals generally similar depth time series and so it is suggested that the observed differences in sediment flux result primarily from differences in the amount of suspended sediment transported into the region of analysis from the inner surf zone (Alsina et al., 2009). While there are differences in the time series of cumulative flux between the two experiments, they are not large. The maximum difference in cumulative flux over the 1-h period presented ($t = 9$–10 h) is only 52 kg/m (at event 132) which is comparable to the sediment transported by the largest single event fluxes recorded over the whole experiment (up to 60 kg/m).

Histograms of event-by-event mass fluxes (Fig. 6a–d, g) indicate that the distribution of fluxes is approximately symmetrical and the results from experiments SB and DR are comparable in the low, mid and upper swash zone. Again, these plots are comparable to those presented by Blenkinsopp et al. (2011), with decreasing maximum flux magnitudes leading to a narrower distribution moving landward, although the range of fluxes is an order of magnitude smaller (±60 kg/event/m compared to a maximum of ±600 kg/event/m in Blenkinsopp et al. (2011) due to the much smaller waves (H_s in Blenkinsopp et al. (2011) was in the range 0.8–3.4 m) and correspondingly shorter swash excursions. Scatter plots comparing the fluxes from matching events in experiment SB and DR (Fig. 6b–e, h) show less scatter than the equivalent bed elevation changes (see Fig. 4b–e and h). This observation provides some support to the idea that while the bed elevation change at a single point on the beach from the same wave may be quite different between the two experiments, the overall effect on the beachface is generally closer and

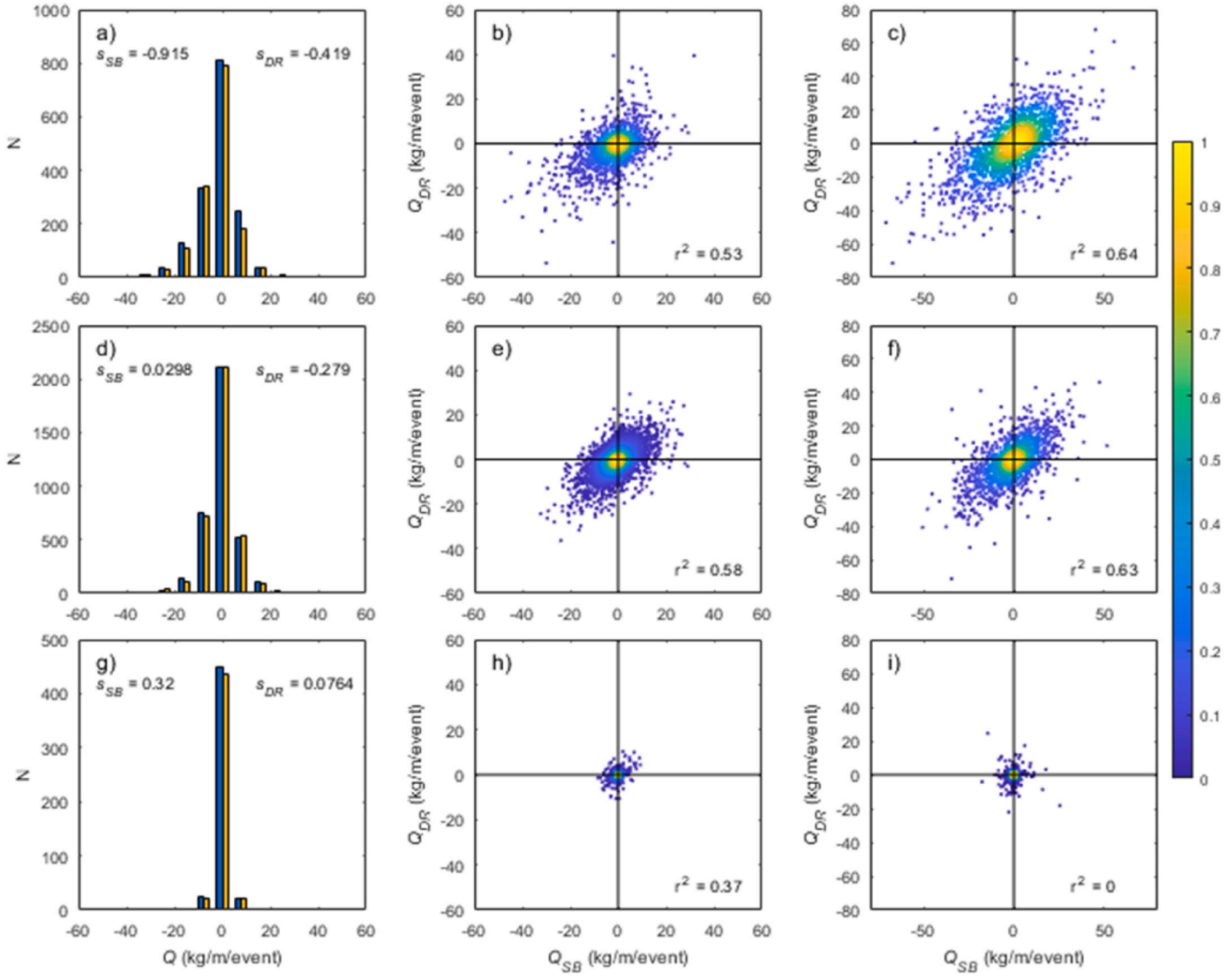

Fig. 6. Left column) Histograms of cross-shore sediment mass flux due to the same swash events for SB (blue) and DR (yellow) at (a) x = 252.4 m, (d) 254.3 m and (g) 258.2 m. Centre column) scatter plots of event-by-event sediment mass flux during SB and DR at (b) x = 252.4I (e) 254.3 m and (h) 258.2 m. Right column) scatter plots of sediment mass flux from infragravity swashes during SB and DR at (c) x = 252.4 m, (f) 254.3 m and (i) 258.2 m. The colour scale indicates the normalised point density.

contributes to the similar overall evolution observed in the two experiments (Fig. 3). For some events, however, the bed response is clearly very different, leading to the outliers in Fig. 6b–e and h and the temporary differences in the time series of cumulative flux at $x = 254.3$ m presented in Fig. 5f.

While event-by-event sediment fluxes are more similar for matching swashes than single point bed elevation changes, there is still considerable scatter which could be expected to lead to differing morphological evolution, or at least different paths to the same quasi-equilibrium profile after many hours. However, it is clear from Fig. 3 that beachface profiles in the two experiments are similar at all times and while morphology changes across the beachface are not the same with every swash, the differences are averaged out over multiple waves. Fig. 6 c, f and i show scatter plots comparing the sediment flux caused by matching infragravity swash events, where infragravity events were determined using a trough-to-trough analysis on the low pass filtered ($f < 0.04$ Hz) shoreline elevation time series. Fig. 6c and f shows that while there is slightly better agreement between flux values from matching infragravity swashes compared to individual swash events, the results remain scattered.

Fig. 7 shows the distribution of bed elevation change over the beachface landward of $x = 248$ m at intervals of 1 and 5 min. Comparing Fig. 7 with Fig. 5, it is evident that as the time over which the bed elevation change is assessed increases from event-by-event to 5-min timescales the influence of divergent transport from individual swash events is reduced and agreement between the cross-shore distributions of bed elevation change in the two experiments improves. Over 5 min, although the cross-shore distribution of changes is quite complex with alternating patterns of accretion and erosion, these patterns are mostly very similar when comparing matching periods in the two experiments (Fig. 7b and d). Over the entire duration of the experiments, the root mean square difference between the experiments is 4.0 mm/min (1-min timescale) and 1.2 mm/min (5-min timescale) with mean absolute errors of 1.8 and 0.7 mm/min respectively, indicating greater agreement between morphology change patterns over the longer 5-min timescale.

Perhaps a more robust method of quantification, is the root mean square transport error (RMSTE) developed by Bosboom et al. (2020) (see Appendix A1). This measure was designed to quantify agreement between morphodynamic model predictions and observations and defines the difference between two morphologies (here the spatial distribution of dz for experiments SB and DR over different timescales) in terms of an optimal sediment transport field, which moves misplaced sediment from the predicted to the observed morphology. This method is much less prone to location errors than more simplistic metrics like RMSE, which reward the underestimation of profile variability and where small errors in the position of features, like sandbars or berms, can lead to large error

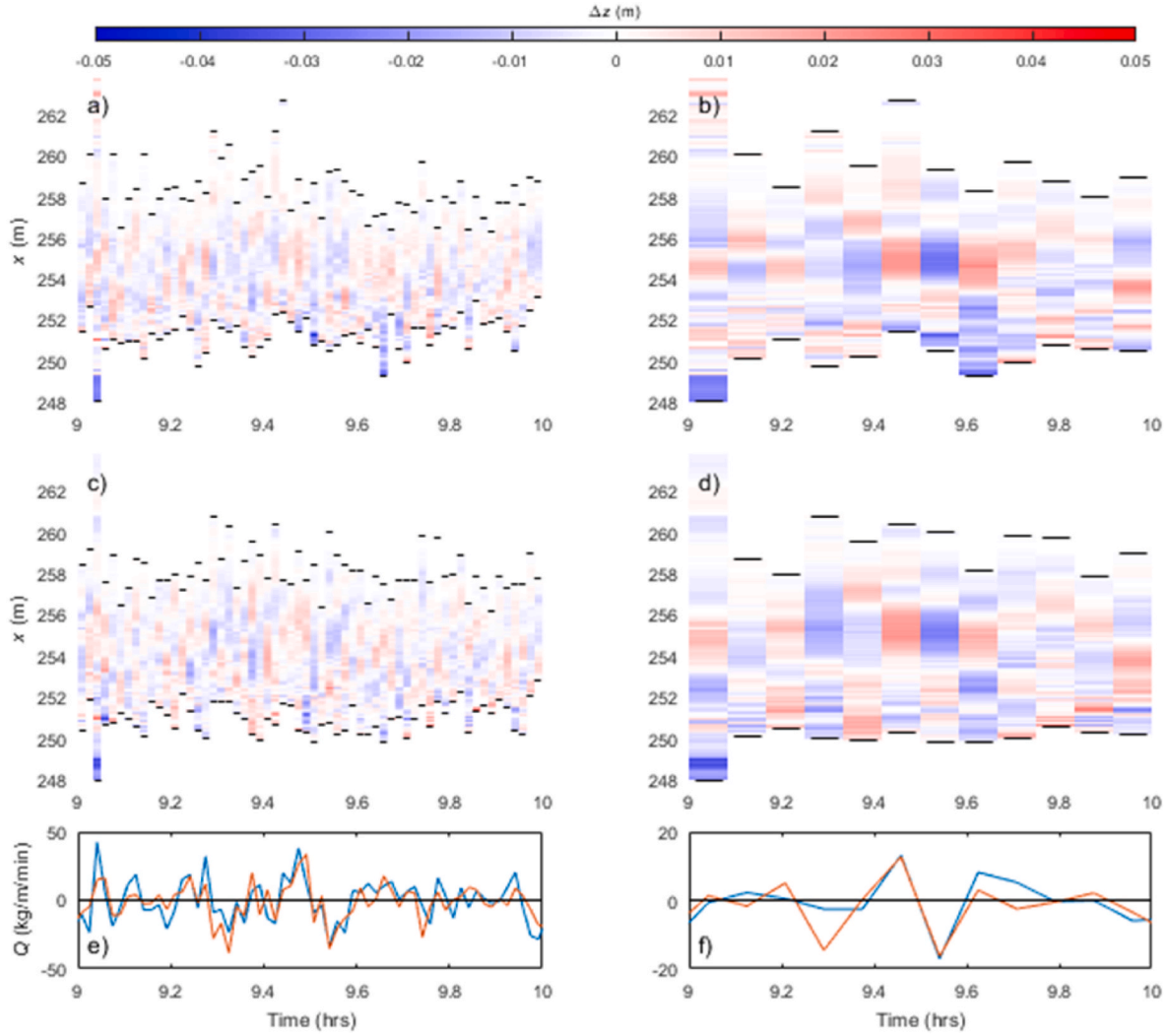

Fig. 7. Cross-shore distribution of bed elevation change in the swash zone over intervals of 1 min (left column) and 5 min (right column) between hours 9 and 10 for experiments (a, b) SB and (c, d) DR. Note that black lines indicate the maximum runup and rundown limits for each interval. (e, f) Mass flux of sediment over each period estimated at x = 254.3 m. Blue line indicates results from experiment SB and red is for DR.

values. The RMSTE between experiments SB and DR for every matching time period throughout the 20-h experiments was calculated using a free seaward boundary which allows for sediment transport across the boundary. Over the entire duration of the experiments, the calculated RMSTE values were 0.0063 m^2/min for the 1-min timescale and 0.0021 m^2/min over 5-min timescales. This again indicates greater agreement between morphological changes over the longer (5-min) time period where short term differences in the cumulative sediment transport due to relatively large differences in transport from individual swashes is smoothed out and has less influence.

Despite the similar patterns observed over 5 min intervals in Fig. 7b and d, there are still differences in the cross-shore sediment flux values from matching periods in SB and DR (Fig. 7f) and a linear regression indicates only a weak correlation ($r^2 = 0.57$) between the 5-min flux values in both experiments over the 20-h duration of the experiment. It is likely that this can be explained by the fact that the cross-shore flux from a single swash can be of the same order of magnitude as that over a period of 5-min and thus any agreement can be negated by a small number of waves with differing behaviour in the two experiments during the period of analysis.

To visualise the temporal and spatial variation of the frequency spectrum of beachface morphology change, spectrograms of the timeseries of bed elevation at all cross-shore locations were calculated for both experiments using a sliding 2-h Hanning window with 98% overlap to coincide with the wave signal repeat period (Fig. 8a and b). To demonstrate the similarity between Experiments SB and DR at different frequencies, a cross-spectrogram between the bed elevation timeseries for the two experiments was also produced using the same parameters as the spectrogram (Fig. 8c). More details of the spectrogram and cross-spectrogram are provided in Appendix A1. Note that due to missing data in Experiment DR, it was not possible to compute the spectrogram for the first 2.5 h and so both experiments are presented from 2.5 h onward for consistency. Repeatable patterns in spectral power with a 2-h period corresponding to the wave repeat period were evident at multiple frequencies, but primarily around 1.25 and 0.5 mHz. Fig. 8a and b presents the cross-shore distribution of power at 1.25 mHz as a function of time. There is evidence of a peak in spectral power in the mid/upper swash zone centred around the mid-point of each 2-h repeat (see solid black line in 8a and b), with lower energy at the start and end of each repeat. This peak is initially between $x = 252.5$ and 255 m and translates landwards as the beachface is eroded in a similar manner for both experiments. The pattern is accentuated in the cross-spectrum at

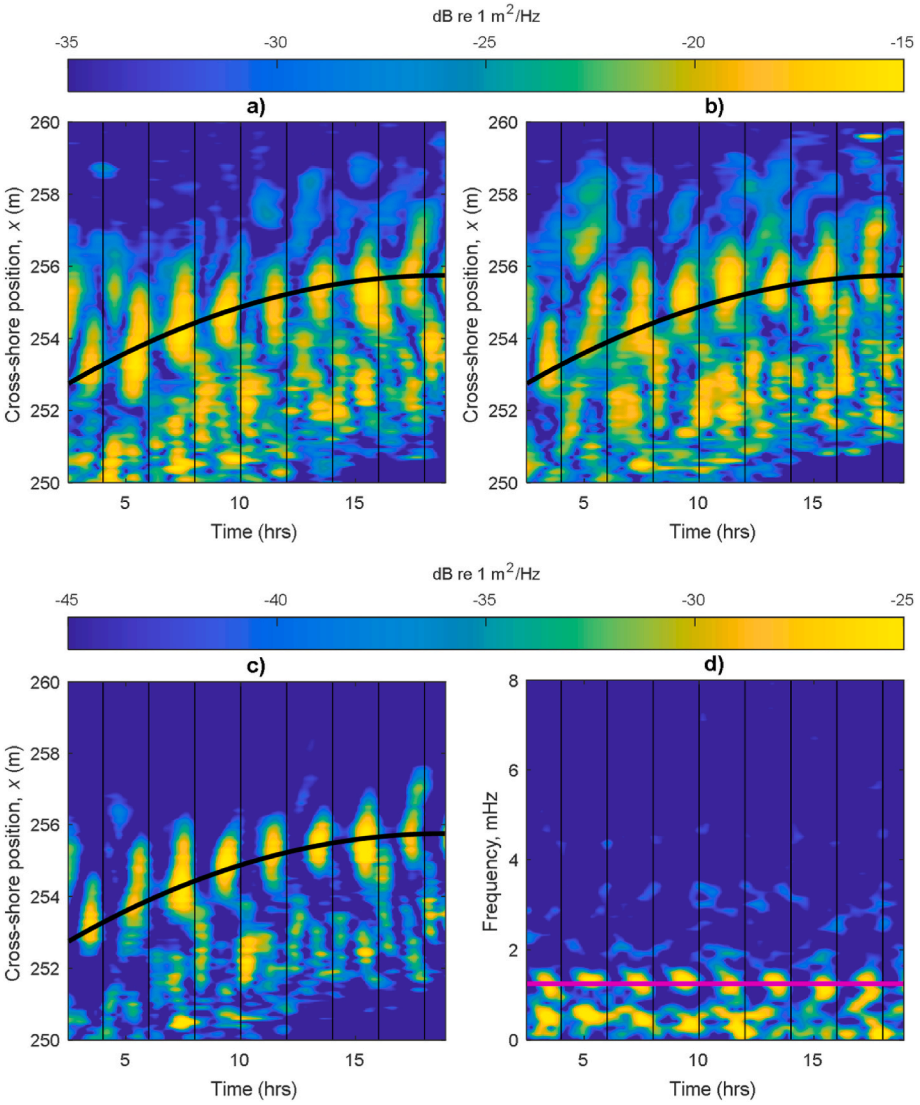

Fig. 8. Top row) Spatial distribution of spectral power at 1.25 mHz as a function of time for a) Experiment SB, and b) Experiment DR. Bottom row: c) Cross-spectrogram between Experiments SB and DR, and d) cross-spectrum extracted along the thick black line in panel c which follows the peaks in spectral power. The horizontal pink line indicates f = 1.25 mHz. The vertical black lines in all panels indicate the start of each 2-h wave signal repeat.

1.25 mHz, indicating the repeatable behaviour of the two experiments at this frequency. The root mean square (RMS) amplitude of the bed elevation change for a particular spectral feature can by estimated by integrating the power spectral density (PSD) over the bandwidth that encompasses that feature. The features observed at 1.25 mHz have an approximate bandwidth of 0.1 mHz and, therefore, from the PSD we estimate the bed variability to be approximately 5 mm RMS. There is also evidence of a further, but less distinct peak in the lower swash zone above the shoreline position. The temporal variation of the cross-spectrum extracted along a line which follows the translation of the spectral peak in Fig. 8a, b, and c is presented in Fig. 8d. Fig. 8d highlights the peaks at 0.5 and 1.25 mHz but there is no evidence of significant energy at higher frequencies approaching the infragravity wave frequency.

3.3. Morphological response to repeated wave forcing

The results presented above indicate that matching swash events have similar flow depth characteristics but there is much less similarity in the corresponding sediment transport flux and bed elevation change indicating limited morphological repeatability at the individual wave timescale. The level of agreement between matching periods of the two experiments increases with longer averaging periods. To gain more insight into morphological repeatability, this section will further explore the morphological response within each experiment to the repeated 2-h wave time series examined in Fig. 8.

Fig. 9a presents a 1-min moving average of the detrended (cubic) bed elevation time series, z_{dt} during the same 30-min period of the repeated wave signal during the 2nd to 10th repeats at $x = 254.3$ m for Experiment SB. Note that Experiment SB is chosen because there are complete measurements for the full 20-h duration with no gaps. The first repeat is not included because the initial planar beach profiles are slightly different and far from quasi-equilibrium and so the initial morphology change during the first 2 h is rapid and shows less consistency between experiments. While the response in the remaining hours is not identical, it is clear that the bed responds in a similar way during each repeat, and particularly during the 2nd to 6th repeats. The level of similarity in Fig. 9a is surprising given that due to the progressive erosion of the bed at this location (see Fig. 3c), the percentage inundation s_{30}, which is used to indicate the relative position within the swash zone varies from 34% for the periods starting at 3h15m and 5h15m to 52% for the period starting at 11h15m. After the 6th repeat, the value of s_{30} at $x = 254.3$ m increases rapidly and the response begins to diverge with the peak value of z_{dt} decreasing from 0.13 m or greater to less than 0.09 m for the 7th to 9th repeats. If the bed elevation is plotted for the cross-shore position corresponding to a constant value of $s_{30} = 34\%$ at each 2-h interval rather than a constant cross-shore location, the bed response, in particular the peak values, becomes more similar for all wave signal repeats (see Fig. 9b). This suggests that using the percentage inundation to indicate relative position within the swash zone is valid. Further evidence for the validity of this method is obtained by comparing depth time series for all repeats at a constant cross-shore position (Fig. 9c) and a constant value of percentage inundation, $s_{30} = 34\%$ (Fig. 9d). At a constant cross-shore position the measured swash depths vary noticeably for the different wave signal repeats (e.g. the peak depth of the same swash event at 17.5 min increases with each repeat) and different

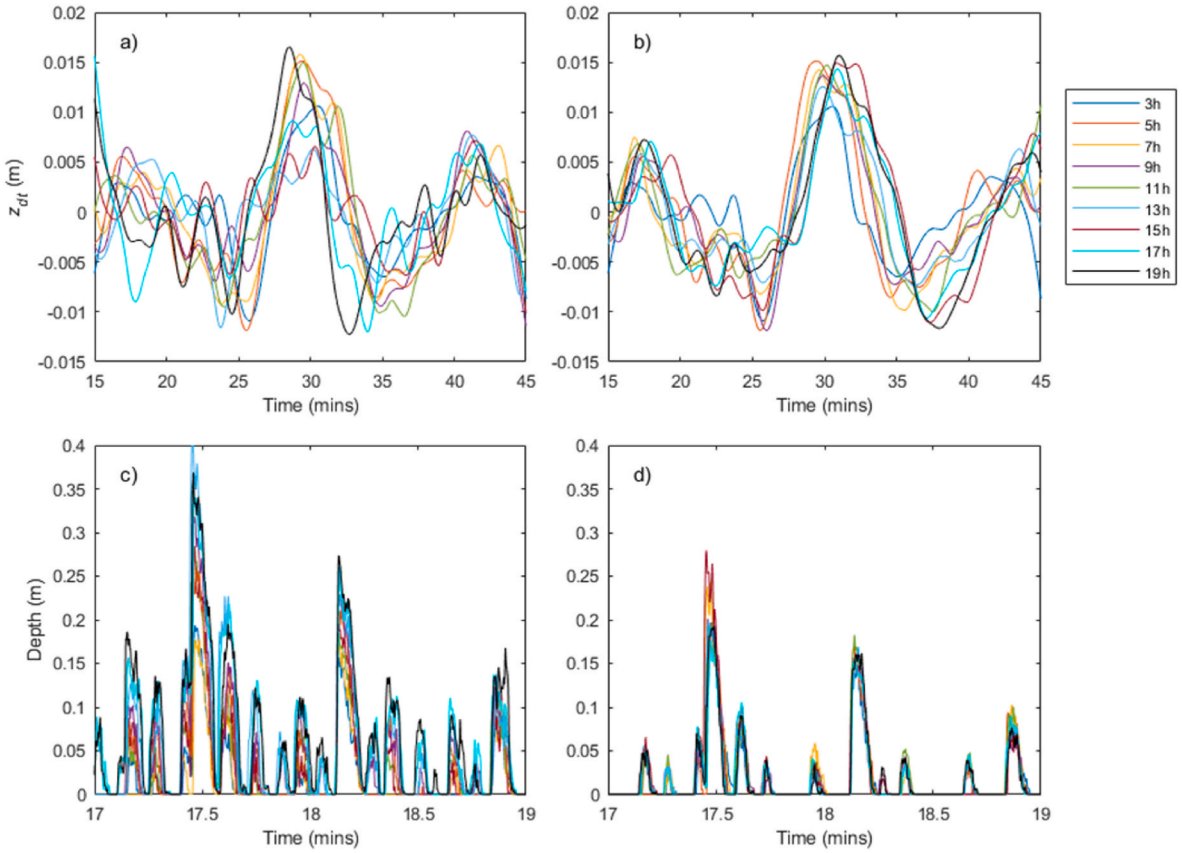

Fig. 9. (Top) 1-min moving average of the detrended bed elevation during the same 30-min period of the repeated wave signal for Phase SB (a) at x = 254.3 m during the 2nd to 6th 10th repeats (corresponding to periods starting a t = 3h15m to 19h15m), and (b) at the cross-shore location where $s_{30} = 34\%$ in each 30-min period during the 2nd to 10th repeats. Times are given as minutes past the odd-numbered hours. (Bottom) Swash depths during a 2-min subsection of each repeat at (c) x = 254.3 m, and (d) the cross-shore location where $s_{30} = 34\%$ in each 30-min period during the 2nd to 10th repeats. The values in the legend represent the start times for each repeat. Note that in all plots the first repeat is not shown as because while it does show similar behaviour, the agreement is substantially less good because the beach is still changing rapidly as it evolves from the initial planar slope.

swash events are measured as the bed erodes and the relative position within the swash zone changes. For a constant value of $s_{30} = 34\%$ (Fig. 9d), the same 12 swash depth peaks are measured during all repeats and the difference in peak depth is smaller than 4 cm except during the event at 17.5 min. The period of the filtered bed elevation oscillation shown in Fig. 9a and b is approximately 12.5 min, which approximately corresponds with the higher frequency peak in the cross-spectrum presented in Fig. 8d of around 1.25 mHz.

Fig. 9b gives some insight into the dynamic nature of beach profile equilibrium. If the beachface is to reach a quasi-equilibrium, we might expect the magnitude of bed response to a repeated 30-min period of waves to reduce over time. This is not evident in Fig. 9b which does not indicate that the variability of the bed elevation decreases with time as the beach gets closer to its quasi-equilibrium profile. We hypothesise that even if quasi-equilibrium were reached, sediment would still be transported in the uprush and backwash of every swash event and lead to perturbations around the quasi-equilibrium profile at timescales ranging from individual waves to many minutes. However, we would expect the net change when measured over the timescale of hours to reduce at an ever-decreasing rate.

Comparable results to those presented in Fig. 9 are obtained when analysing any subsection of the 2-h repeats. Autocorrelation of detrended bed elevation data at $x = 254.3$ m from experiment SB indicates peaks in the autocorrelation function at lags of ±2 h (0.39), ±4 h (0.24), ±6 h (0.15) and ±8 h (0.12) and similar results can be obtained at all locations within the low and mid swash region ($x = 252$–258 m). Cross correlation of the bed elevation data from experiments SB and DR provides similar results with peaks at 0 h (0.57), +2 h (0.4), −2 h (0.33), +4 h (0.28), −4 h (0.17) and +6 h (0.15) which further supports the observations in section 3.2 that the beachface evolution in the two experiments follows a similar pattern.

Fig. 10 presents histograms of the wave-by-wave sediment mass net flux for Experiment SB during each 2-h repeat at a constant relative position in the swash zone corresponding to $x = 254.3$ m during the first 2-h ($s_{120} = 29\%$). Fig. 10 also details the net (ΔM_{net}) and gross (ΔM_{abs}) beachface mass change per metre width during each 2-h period. Here the gross mass change is calculated by summing the absolute values of all swash-by-swash mass changes measured during the analysis period and gives an indication of the amount of sediment being transported past a location on the beachface in either the landward or seaward direction.

Fig. 10 indicates that the total number of swash events detected in each 2-h period is similar, except during the first 2-h. The distribution of measured fluxes during each repeat is approximately symmetrical, as observed for the whole experimental period in Fig. 6a–d, g. However, there is a clear difference in the distribution of fluxes during the first 6 h ($t = 0$–6 h) and the last 14 h ($t = 6$–20 h). The first 6 h correspond to the period when the initially planar beachface is reshaped and the most rapid changes in bar crest elevation and position and overall beach volume occur (Fig. 2) and there is evidence of a larger proportion of large mass fluxes (>±7.5 kg/event/m). After $t = 6$ h, there is an increase in the percentage of fluxes smaller than ±2.5 kg/event/m and a corresponding decrease in the percentage of larger fluxes. During the last 14 h, the histograms for each 2-h period are very similar, with a slowly increasing majority of events leading to net mass fluxes in the range ±2.5 kg/event/m and slightly more events causing negative fluxes with a magnitude greater than 2.5 kg/event/m than positive fluxes in this range, leading to consistent erosive trend indicated by the negative net change in beachface mass (ΔM_{net}) during all repeats. An almost identical result is obtained for experiment DR for $s_{120} = 29\%$, and the observed trend with time is common at all locations in the low and mid swash zone, but not the upper swash where relatively few events are measured.

At the chosen constant relative position ($s_{120} = 29\%$), the values of net beachface mass change appear to become less variable with time, but there is only weak evidence of decreasing values. By contrast, the gross changes are notably larger during the first 6 h before settling to a consistent value of approximately 1 100 kg/m every 2-h during the remainder of the experiment. Consistent with previous studies, the gross change in beachface mass during all periods is an order of magnitude larger than the net change, (Blenkinsopp et al., 2011; Ruessink et al., 2015).

The results presented in Fig. 10 demonstrate that throughout the experiment, substantial quantities of sediment can be transported with every wave, leading to large values of gross mass change (ΔM_{abs}). While the values of ΔM_{abs} remain large, they are observed to decrease by around 30% after the bulk of primary bar formation has occurred at around $t = 6$ h. This decrease is primarily the result of a reduction in the number of swash events causing mass fluxes of sediment larger than ±7.5 kg/event/m. To illustrate this, individual mass flux events larger than ±7.5 kg/event/m account for more than 40% of the comparatively large gross change values during the first 6 h, but less than 32% during the final 14 h. It is speculated that the reduction in the number of larger events may be due to influence of the primary bar which grows substantially during the first 6-h and partially controls the wave energy reaching the shoreline. The effect of the initial bar growth on swash hydrodynamics is illustrated in Fig. 11 which shows a clear decay of significant swash excursion (X_s) and height (S) as the beach profile evolves closer to a quasi-equilibrium condition, with the most rapid decay occurring during the first 6-h. Here X_s and S are calculated as four times the standard deviation of the horizontal and vertical shoreline time series respectively. The observed reduction in swash as the bar develops may lead to a reduction in the sediment transport capacity of equivalent swash events or closer intra-swash balance between uprush and backwash sediment transport, though it is acknowledged that steepening of the beachface will also reduce X_s and S.

Overall, it appears that as the beach gets closer to quasi-equilibrium, the swash zone morphology remains very dynamic with gross changes that decrease with time but remain large. However, the chance of a single swash event causing a substantial change in beachface mass reduces and this likely leads to a smaller likelihood of large net change.

4. Repeatability and consequences for coastal researchers and practitioners

The results presented in Section 3 demonstrate that in a large-scale two-dimensional laboratory setting, a beach will respond in almost the same way when exposed to the same forcing over timescales of several minutes (e.g., see Fig. 7 b, d, f). Thus, sediment transport on beaches, even in the highly energetic and variable swash zone displays a level of determinism which gives confidence in the results from physical modelling studies. When comparing almost identical experiments, unavoidable differences in turbulence and small-scale morphodynamic feedback mean that the exact nature of swash hydrodynamics and hence sediment transport will vary at all timescales from one experiment to another and can lead to short-term differences in morphological response. However, there is no evidence of morphodynamic feedback leading to sustained differences in morphology; short-term differences typically negated quickly by subsequent waves and beach profiles remain similar throughout. This result is compatible with the conclusions of Blenkinsopp et al. (2011) who found from field measurements that despite the existence of individual swash events that can cause fluxes of sediment that are comparable to those observed on a tidal time scale, frequent reversals in transport direction act to limit net transport such that the beach face volume does not rapidly erode or accrete. As a result, beachface morphology change in energetic conditions occurred as a result of a balance of onshore and offshore fluxes at the inter-swash timescale over sequences of multiple swash events.

While a quasi-equilibrium profile was not achieved in the 20-h duration experiments reported here, the experimental results support the concept that a beach will approach a consistent profile under a given wave forcing. This quasi-equilibrium condition is dynamic and is constantly perturbed by individual or groups of waves, but the underlying stability of the profile means that these perturbations are damped

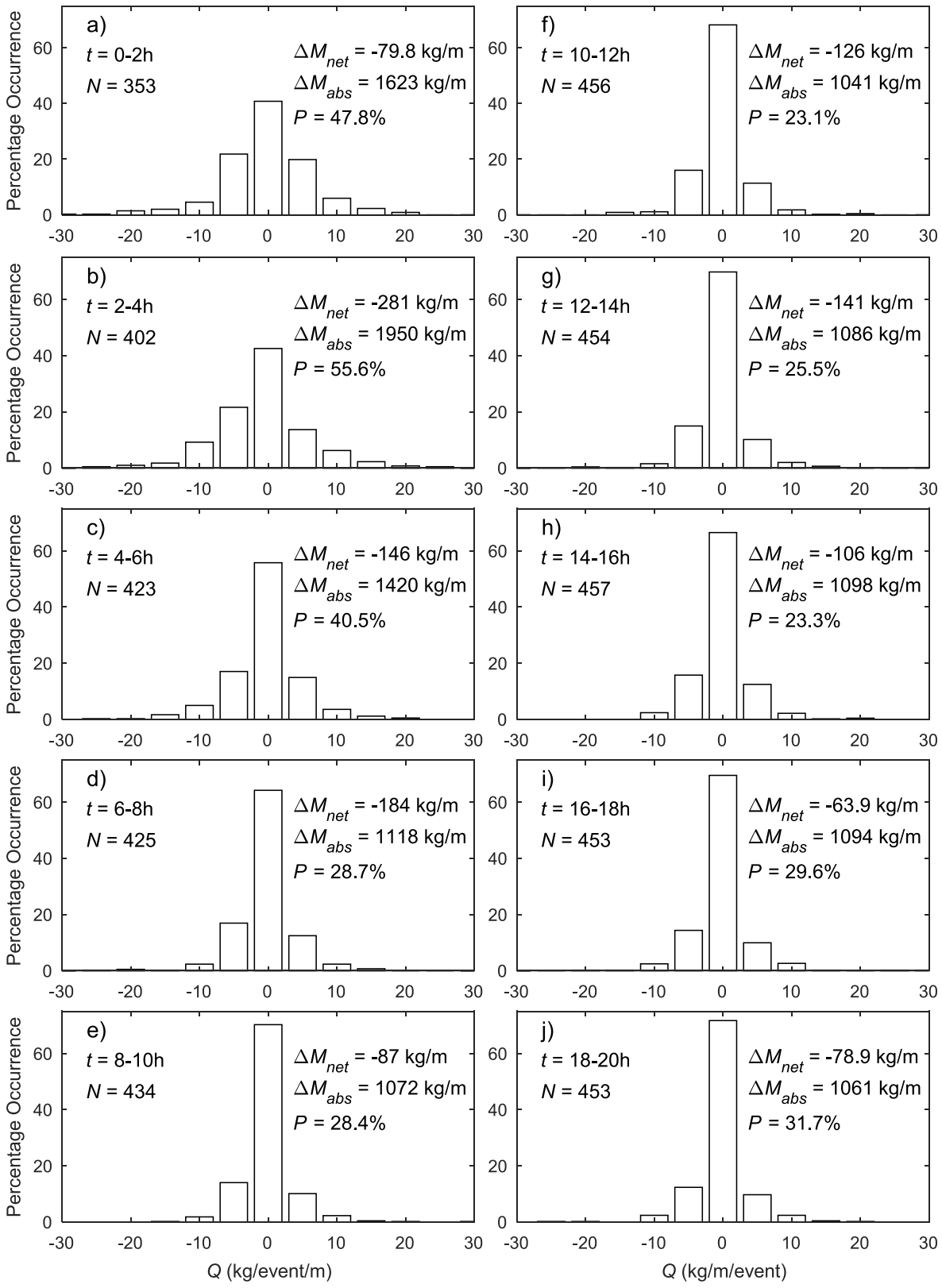

Fig. 10. (a to f) Histograms of the cross-shore net mass flux due to every detected swash event at a constant relative position in the swash zone ($s_{120} = 29\%$) during each 2-h repeat of the wave signal for Experiment SB. $s_{120} = 29\%$ corresponds to x = 254.3 m during the first 2- hour period. N indicates the number of swash events detected and P is the percentage of gross volume change caused by single event fluxes larger than ±7.5 kg/m/event.

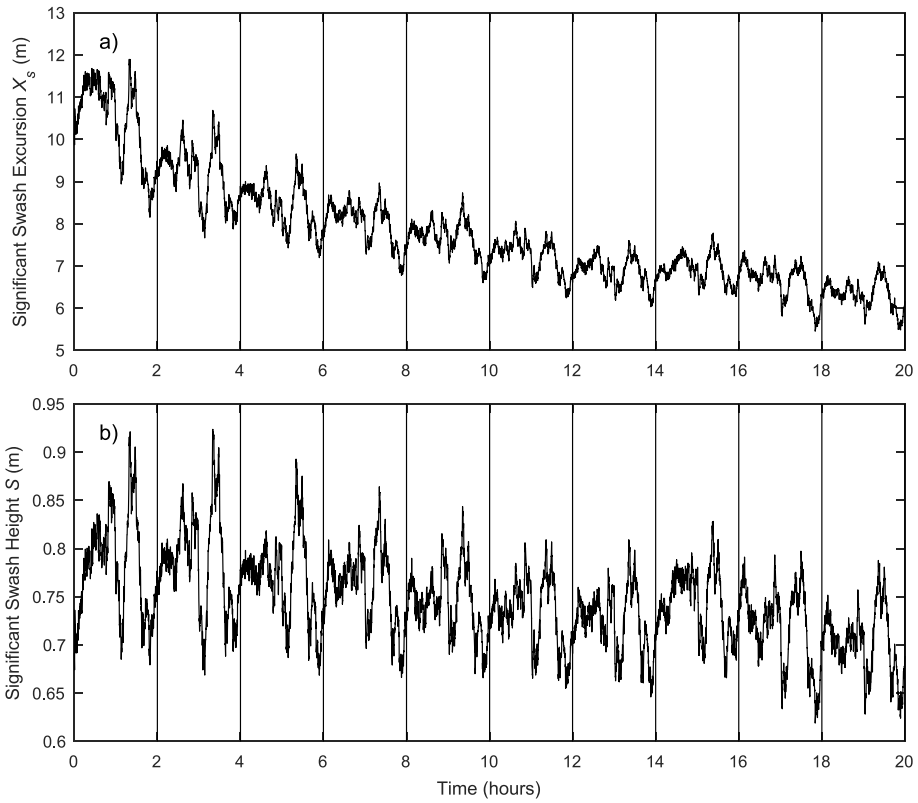

Fig. 11. Time series of (a) significant horizontal swash excursion and (b) significant swash height calculated in a moving 10-min window through the experiment duration.

out over time with the equilibrium profile acting as an attractor. If large enough, the perturbations could potentially influence conclusions drawn from intermittent beach profile measurements. For the current data however, the 90th percentile range of bed elevation within a moving 5-min window is smaller than ±0.02 m. This value is comparable to the vertical accuracy of the mechanical profiler or typical RTK GPS and so a measured beach profile can be considered representative and not significantly influenced by short-term perturbations.

While the results have demonstrated that a repeated experiment on a sand profile leads to the same beach profile, the beach profile changes on a wave-by-wave basis do not match. This highlights the challenge of modelling sediment transport precisely at the wave-by-wave timescale and for engineering purposes, modelling should focus on correct prediction of the statistics of wave-by-wave sediment fluxes to ensure that the time-averaged distribution of sediment flux $q(x)$ is correct at the wave-group timescale or greater. Thus, the wave-group resolving approach of the original XBeach storm erosion model (Roelvink et al., 2009) or models which predict $q(x)$ based on the disequilibrium in the time-averaged wave energy flux and beach gradient such as the ForCE model (Davidson, 2021) appear to represent efficient, practical approaches depending on the timescale of interest.

5. Conclusions

The response of a large-scale laboratory beach with the same initial state to multiple repeats of the same wave forcing has been investigated to gain insight into the repeatability of morphological change over timescales from individual swash events to hours. Two identical experiments were conducted in a large-scale 2D wave flume using a sand beach with an initially 1:10 planar beach slope subjected to 10 repeats of the same 2-h irregular wave timeseries. Swash zone hydrodynamics and morphology were captured at 25 Hz using a laser scanner array and in addition, complete beach profiles were obtained at regular intervals ranging from 20 min to 3 h.

The results indicated that bed elevation change and cross-shore sediment flux are not consistent for matching individual swash events, despite comparable flow depth timeseries. In common with previous experimental results, small numbers of individual swash events were found to transport large quantities of sediment and cause significant (several centimetres), but short-lived differences in bed elevation between the two experiments, however these differences were cancelled out by subsequent waves. Over longer timescales containing several infragravity swash periods however (e.g., 5 min and more), fluxes were found to be reasonably consistent in direction, magnitude and spatial distribution in the cross-shore direction.

The rate of morphology change was observed to slow as the experiment progressed, indicating the approach to a quasi-equilibrium profile, though even after 20 h the rate of change of beach volume did not approach zero. Despite the reduction in net transport with time, the gross swash zone sediment transport remained high throughout the experiment, though the proportion of swash events causing large sediment fluxes (>±7.5 kg/event/m) reduced.

Over periods greater than 20 min, the complete beach profile data indicated very similar morphology change over the whole cross-section, with the RMS difference between profiles remaining almost the same as the value after initial construction throughout the experiments. It can be concluded that at the resolution of typical morphology measurements, laboratory beach profiles are repeatable over timescales encompassing multiple infragravity wave periods, providing confidence in the results of physical modelling studies of beach response.

Funding

This project received funding from the European Union's Horizon 2020 research and innovation programme under grant agreement No 654110, HYDRALAB+. P. Bayle was supported by a PhD scholarship

through the EPSRC CDT in Water Informatics: Science & Engineering (WISE). A. Hunter was supported by a University of Bath Alumni Fund grant. T. Baldock acknowledges support from the Australian Research Council through Discovery grant DP140101302.

CRediT authorship contribution statement

Chris E. Blenkinsopp: Conceptualization, Data curation, Formal analysis, Funding acquisition, Investigation, Methodology, Project administration, Resources, Software, Supervision, Visualization, Writing – original draft. **Alan J. Hunter:** Formal analysis, Investigation, Methodology, Resources, Software, Visualization, Writing – review & editing. **Tom E. Baldock:** Conceptualization, Funding acquisition, Investigation, Methodology, Writing – review & editing. **Paul M. Bayle:** Formal analysis, Investigation, Methodology, Software, Writing – review & editing. **Judith Bosboom:** Formal analysis, Writing – review & editing. **Daniel Conley:** Conceptualization, Funding acquisition, Investigation, Methodology, Resources, Supervision. **Gerd Masselink:** Conceptualization, Funding acquisition, Investigation, Methodology, Resources, Supervision, Writing – review & editing.

Declaration of competing interest

The authors declare that they have no known competing financial interests or personal relationships that could have appeared to influence the work reported in this paper.

Data availability

Post-processed experimental data that support the findings of this study are openly available from the zenodo repository at https://doi.org/10.5281/zenodo.388979.

Acknowledgments

The authors wish to acknowledge the support of the DynaRev experiment team including Emily Gulson, Isabel Kelly, Rafael Almar, Ian Turner, Tomas Beuzen, Robert McCall, Huub Rijper, Ad Reniers, Peter Troch, David Gallach-Sanchez, Oscar Bryan, Gwyn Hennessey, Peter Ganderton, Marion Tissier, Matthias Kudella, Stefan Schimmels, Aaron Bennett, Jak McCarroll and all the GWK staff.

Appendix A. Data analysis methods

A1 Root Mean Square Transport Error (RMSTE)

This paper uses both the root-mean squared bathymetric error (RMSE) and the root-mean-squared transport error (RMSTE) proposed by Bosboom et al. (2020) as error metrics. Unlike the RMSE, the RMSTE detects misplacement distances of predicted features. Also, the RMSTE avoids the tendency of the RMSE to reward underprediction of variability, known as the double penalty effect.

In Equation (A1.1), z_{SB} and z_{DR} are the observed bed levels at each cross-shore location x over the domain Ω. If $e = z_{DR} - z_{SB}$ is the point-wise bathymetric error, the root-mean-squared bathymetric error (RMSE) is defined as:

$$\mathrm{RMSE} = \frac{1}{\sqrt{A_\Omega}}\left(\int_{x\in\Omega} |z_{DR}(x) - z_{SB}(x)|^2 \mathrm{d}x\right)^{1/2} = \frac{1}{\sqrt{A_\Omega}}\|e\| \tag{A.1}$$

with A_Ω the domain surface area. Similarly, we can define the root-mean-squared transport error (RMSTE) as the root-mean-square of a quadratic optimal transport field q that transports misplaced sediment from z_{SB} to z_{DR} at the "cheapest" cost:

$$\mathrm{RMSTE} = \left(\frac{1}{A_\Omega}\int_{x\in\Omega} |q(x)|^2 \mathrm{d}x\right)^{1/2} = \frac{1}{\sqrt{A_\Omega}}\|q\| \tag{A.2}$$

The optimal transport field q, which is to be interpreted as a transport difference field between z_{SB} and z_{DR}, is obtained by solving a Poisson equation. When using free boundaries, which are part of the transport optimisation, a bias is allowed to exist between the two bathymetric fields. In 1D, the determination of the optimal transport $q(x)$ with free boundaries at both ends of the domain is equivalent to straightforward numerical integration of the volume balance while requiring $\overline{q} = 0$.

For the 1D application presented in section 3.2, RMSTE is determined as $\mathrm{RMSTE} = \sqrt{\overline{q(x)}^2}$, with $q(x)$ over matching 1 and 5-min intervals.

Appendix A2. Spectrogram and Cross-spectrogram

Spectral analysis of the timeseries of bed elevation for both experiments $z_{SB}(t,x)$ and $z_{DR}(t,x)$ is presented in section 3.2 where t represents time and x cross-shore position. These timeseries were de-trended in time to prevent leakage of the dominant spectral power close to zero frequency from obscuring features of interest using a 5th order polynomial fit. The cross-spectrogram was computed using short-time Fourier transforms (STFTs), i.e.,

$$\mathrm{S}_{\mathrm{m,n}}(\tau,f,x) = \left|S_m(\tau,f,x)S_n^*(\tau,f,x)\right| \tag{A.3}$$

where

$$S_n(\tau,f,x) = \int_{-T/2}^{T/2} w(t)\ \widehat{z_n}(t+\tau,x)\ \exp(-j2\pi f\ t)\ \mathrm{d}t \tag{A.4}$$

is the STFT of $z_n(t,x)$ and $w(t)$ is a temporal window of duration T. For the cross-spectrogram, $z_m = z_{SB}$ and $z_n = z_{DR}$. The spectrogram for each experiment is obtained using eq. A.4 with $m = n$. This was implemented using Matlab's xspectrogram function with a Hanning window of 2-h duration in the present study.

References

Alsina, J.M., Falchetti, S., Baldock, T.E., 2009. Measurements and modelling of the advection of suspended sediment in the swash zone by solitary waves. Coast. Eng. 56, 621–631. https://doi.org/10.1016/j.coastaleng.2009.01.007.

Alsina, J.M., Cáceres, I., 2011. Sediment suspension events in the inner surf and swash zone. Measurements in large-scale and high-energy wave conditions. Coast. Eng. 58, 657–679. https://doi.org/10.1016/j.coastaleng.2011.03.002.

Alsina, J.M., Cáceres, I., Brocchini, M., Baldock, T.E., 2012. An experimental study on sediment transport and bed evolution under different swash zone morphological conditions. Coast. Eng. 68, 31–43. https://doi.org/10.1016/j.coastaleng.2012.04.008.

Alsina, J.M., Padilla, E.M., Cáceres, I., 2016. Sediment transport and beach profile evolution induced by bi-chromatic wave groups with different group periods. Coastal Engineering 114.

Alsina, J.M., van der Zanden, J., Caceres, I., Ribberink, J.S., 2018. The influence of wave groups and wave-swash interactions on sediment transport and bed evolution in the swash zone. Coast. Eng. 140, 23–42. https://doi.org/10.1016/j.coastaleng.2016.04.020.

Baldock, T.E., Alsina, J.A., Vicinanza, D., Contestabile, P., Power, H., Sanchez-Arcilla, A., 2011. Large-scale experiments on beach profile evolution and surf and swash zone sediment transport induced by long waves, wave groups and random waves. Coast. Eng. 58, 214–227. https://doi.org/10.1016/j.coastaleng.2010.10.006.

Baldock, T.E., Birrien, F., Atkinson, A., Shimamoto, T., Wu, S., Callaghan, D.P., Nielsen, P., 2017. Morphological hysteresis in the evolution of beach profiles under sequences of wave climates - Part 1; observations. Coast. Eng. 128, 92–105. https://doi.org/10.1016/j.coastaleng.2017.08.005.

Bayle, P.M., Beuzen, T., Blenkinsopp, C.E., Baldock, T.E., Turner, I.L., 2021. A new approach for scaling beach profile evolution and sediment transport rates in distorted laboratory models. Coast. Eng. 163, 103794 https://doi.org/10.1016/j.coastaleng.2020.103794.

Bayle, P.M., Blenkinsopp, C.E., Conley, D.C., Masselink, G., Beuzen, T., Almar, R., 2020. Performance of a dynamic cobble berm revetment for coastal protection, under increasing water level. Coast. Eng. 159, 103712 https://doi.org/10.1016/j.coastaleng.2020.103712.

Beuzen, T., Turner, I.L., Blenkinsopp, C.E., Atkinson, A., Flocard, F., Baldock, T.E., 2018. Physical model study of beach profile evolution by sea level rise in the presence of seawalls. Coast. Eng. 136, 172–182.

Birrien, F., Atkinson, A., Shimamoto, T., Baldock, T.E., 2018. Hysteresis in the evolution of beach profile parameters under sequences of wave climates - Part 2; Modelling. Coast. Eng. 133, 13–25. https://doi.org/10.1016/j.coastaleng.2017.12.001.

Blenkinsopp, C.E., Bayle, P.M., Conley, D.C., Masselink, G., Gulson, E., Kelly, I., Almar, R., Turner, I.L., Baldock, T.E., Beuzen, T., McCall, R.T., Rijper, H., Reniers, A., Troch, P., Gallach-Sanchez, D., Hunter, A.J., Bryan, O., Hennessey, G., Ganderton, P., Tissier, M., Kudella, M., Schimmels, A., 2021. High-resolution, large-scale laboratory measurements of a sandy beach and dynamic cobble berm revetment. Sci. Data 8, 22. https://doi.org/10.1038/s41597-021-00805-1.

Blenkinsopp, C.E., Turner, I.L., Masselink, G., Russell, P.E., 2011. Swash zone sediment fluxes: field observations. Coast. Eng. 58, 28–44. https://doi.org/10.1016/j.coastaleng.2010.08.002.

Bosboom, J., Mol, M., Reniers, A., Stive, M.J.F., de Valk, C.F., 2020. Optimal sediment transport for morphodynamic model validation. Coast. Eng. 158, 103662 https://doi.org/10.1016/j.coastaleng.2020.103662.

Bruun, P., 1954. Use of small-scale experiments with equilibrium profiles in studying actual problems and developing plans for coastal protection. Eos, Transactions American Geophysical Union 35, 445–452. https://doi.org/10.1029/TR035i003p00445.

Caceres, I., Alsina, J.A., 2016. Suspended sediment transport and beach dynamics induced by monochromatic conditions, long waves and wave groups. Coast. Eng. 108, 36–55. https://doi.org/10.1016/j.coastaleng.2015.11.004.

Cáceres, I., Alsina, J.M., 2012. A detailed, event-by-event analysis of suspended sediment concentration in the swash zone. Continent. Shelf Res. 41, 61–76. https://doi.org/10.1016/j.csr.2012.04.004.

Davidson, M., 2021. Forecasting coastal evolution on time-scales of days to decades. Coast. Eng. 168, 103928 https://doi.org/10.1016/j.coastaleng.2021.103928.

Dean, R.G., 2005. Dynamic equilibrium of beaches. In: Schwartz, M.L. (Ed.), Encyclopedia of Coastal Science. Encyclopedia of Earth Science Series. Springer, Dordrecht. https://doi.org/10.1007/1-4020-3880-1_129.

Dette, H.H., Larson, M., Murphy, J., Newe, J., Peters, K., Reniers, A., Steetzel, H., 2002. Application of prototype flume tests for beach nourishment assessment. Coast. Eng. 47, 137–177. https://doi.org/10.1016/S0378-3839(02)00124-2.

Eichentopf, S., 2020. Beach Morphodynamics under Sequences of High and Low Energy Wave Conditions. PhD Thesis. Imperial College, London.

Eichentopf, S., Cáceres, I., Alsina, J.M., 2018. Breaker bar morphodynamics under erosive and accretive wave conditions in large-scale experiments. Coast. Eng. 138, 36–48. https://doi.org/10.1016/j.coastaleng.2018.04.010.

Eichentopf, S., van der Zanden, J., Cáceres, I., Alsina, J.M., 2019. Beach profile evolution towards equilibrium from varying initial morphologies. J. Mar. Sci. Eng. 7, 406. https://doi.org/10.3390/jmse7110406.

Hughes, M.G., Moseley, A.S., 2007. Hydrokinematic regions within the swash zone. Continent. Shelf Res. 27, 2000–2013. https://doi.org/10.1016/j.csr.2007.04.005.

Johnson, D.W., 1920. Shore processes and shore-line development. Geogr. J. 55.

Larson, M., 1988. Quantification of Beach Profile Change. Lund University.

Larson, M., Kraus, N.C., 1989. SBeach: Numerical Model for Simulating Storm-Induced Beach Change; Report 1: Empirical Foundation and Model Development. Technical Report - US Army Coastal Engineering Research Center, 89-9.

Masselink, G., Ruju, A., Conley, D., Turner, I.L., Ruessink, G., Matias, A., Thompson, C., Castelle, B., Puleo, J., Citerone, V., Wolters, G., 2016. Large-scale barrier dynamics experiment II (BARDEX II): experimental design, instrumentation, test program, and data set. Coast. Eng. 113, 3–18. https://doi.org/10.1016/j.coastaleng.2015.07.009.

O'Donoghue, T., Kikkert, G.A., Pokrajac, D., Dodd, N., Briganti, R., 2016. Intra-swash hydrodynamics and sediment flux for dambreak swash on coarse-grained beaches. Coast. Eng. 112, 113–130. https://doi.org/10.1016/j.coastaleng.2016.03.004.

Roelvink, D., Reniers, A., van Dongeren, A., van Thiel de Vries, J., McCall, R., Lescinski, J., 2009. Modelling storm impacts on beaches, dunes and barrier islands. Coast. Eng. 56, 1133–1152. https://doi.org/10.1016/j.coastaleng.2009.08.006.

Ruessink, B.G., Blenkinsopp, C.E., Brinkkemper, J.A., Castelle, B., Dubarbier, B., Grasso, F., Puleo, J.A., Lanckriet, T., 2015. Sandbar and beach-face evolution on a prototype coarse sandy barrier. Coast. Eng. 113, 19–32. https://doi.org/10.1016/j.coastaleng.2015.11.005.

Sutherland, J., Peet, A.H., Soulsby, R.L., 2004a. Evaluating the performance of morphological models. Coast. Eng. 51, 917–939. https://doi.org/10.1016/j.coastaleng.2004.07.015.

Sutherland, J., Walstra, D.J.R., Chesher, T.J., van Rijn, L.C., Southgate, H.N., 2004b. Evaluation of coastal area modelling systems at an estuary mouth. Coast. Eng. 51, 119–142. https://doi.org/10.1016/j.coastaleng.2003.12.003.

van der Zanden, J., Alsina, J.A., Caceres, I., Buijsrogge, R.H., Ribberink, J.S., 2015. Bed level motions and sheet flow processes in the swash zone: observations with a new conductivity-based concentration measuring technique (ccm+). Coast. Eng. 105, 47–65. https://doi.org/10.1016/j.coastaleng.2015.08.009.

van der Zanden, J., Caceres, I., Eichentopf, S., Ribberink, J.S., ven der Werf, J.J., Alsina, J.M., 2019. Sand transport processes and bed level changes induced by two alternating laboratory swash events. Coast. Eng. 152, 103519 https://doi.org/10.1016/j.coastaleng.2019.103519.

van Rijn, L.C., Walstra, D.J.R., Grasmeiher, B., Sutherland, J., Pan, S., Sierra, J.P., 2003. The predictability of cross-shore bed evolution of sandy beaches at the time scale of storms and seasons using process-based profile models. Coast. Eng. 47, 295–327. https://doi.org/10.1016/S0378-3839(02)00120-5.